# CHIRAL WOODPILE MORPHOLOGY OPTIMIZATION FOR PLASMONIC ENHANCED ENANTIOMERIC DETECTION IN PHARMACOLOGY QUALITY MANAGEMENT

**Gautam Ramasamy**

*Anglo-Chinese School (International) Singapore, Institute of High Performance Computing, A\*STAR (Agency for Science, Technology and Research), Republic of Singapore*
*gautam.ramasamy@acsinternational.com.sg*

**Eng Huat Khoo**

*Electronics and Photonics Department, Institute of High Performance Computing, A\*STAR (Agency for Science, Technology and Research), National University of Singapore, Nanyang Technological University (Singapore), Harvard University (United States), Republic of Singapore*
*khooeh@ihpc.a-star.edu.sg*

## Abstract

*The majority of pharmaceuticals currently in circulation are chiral compounds; mostly sold as equimolar mixtures of two enantiomers. Albeit, they have identical chemical structures, the human body metabolizes each enantiomer by separate pathways due to their different handedness. Hence, one isomer may exhibit the intended pharmaceutical effect, whereas the other exists as an inactive impurity or, occasionally, may engender undesirable side-effects and toxicity, like in the Softenon disaster which caused circa one thousand congenital disabilities (International Union of Crystallography, 2016). Therefore, it is imperative to promote chiral separation and analysis of chiral drugs in pharmaceutical manufacture to eliminate the undesirable enantiomer (Nguyen, He, & Pham-Huy, 2006).*

*Recently, plasmonic-enhanced metamaterials have been shown to amplify the subtle circular dichroic effects of chiral molecules by many orders of magnitude, making enantioselective assays more precise by amplifying the CD signal, enabling discrimination of nuanced spectral features, never seen before (Nguyen et al., 2006). This paper advances the sensitivity of CD spectroscopy by studying a newly designed chiral woodpile nanostructure that uses plasmon-generated superchiral near fields to enhance the dissymmetry of chiral molecules and magnify their chiroptical effects. Simulated to outperform gammadion arrays proposed by competitor papers by 1206 %, it empowers increased measurement precision in the assessment of enantiomeric excess in the quality management of drug manufacture, increasing safety. Furthermore, it may potentially lead to earlier detection of diseases such as HIV and other viruses. Lastly, for the first time, this paper proposes a revolutionary but intuitive mechanism to explain the generation of the superchiral near field of a plasmonic-enhanced nanostructure. Shown to corroborate with simulation, it provides a more profound understanding of the underlying mechanisms beyond just the 'plasmon-plasmon coupling' which preceding works have already discussed. This knowledge opens up new avenues to develop nanostructures with even stronger circular dichroic properties.*

**Keywords**

Chiral Woodpile Nanostructure, Circular Dichroism Spectra, Superchiral Field, Plasmonic Interaction
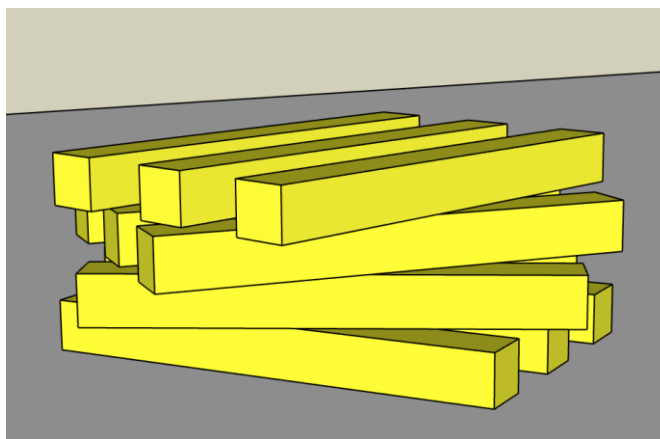
# 1. Introduction



**Figure 1:** *4-Layered Chiral Woodpile Nanostructure*

The interaction between chiral molecules and plasmonic nanostructures enhances their absorption, which makes circular dichroism (CD) spectroscopy a sensitive chirality detection method (Maoz et al., 2013). Although there is a lack of experimental support to pinpoint the mechanism behind CD induction, a plethora have been proposed; plasmon-plasmon interaction (Kuzyk, 2012), plasmon-molecule Coulomb interaction (Fan, & Govorov, 2011), coupling of electron wave functions of molecule and nanoparticle (Xia, Zhou, & Tang, 2011), among others.

For a nanostructure to show strong circular dichroic effects, it must preferentially absorb either right circularly polarized light (RCPL) or left circularly polarized light (LCPL) over the other. This necessitates a chiral structure which interacts differently with RCPL and LCPL, which are themselves chiral.

In pondering about the simplest chiral structure conceivable, a specially designed a chiral assembly called a woodpile structure was designed (see Figure 1). It is constructed by arranging straight nanowires, with a square cross-sectional area, parallel to one another, and stacking multiple layers of these, rotated at incrementally different angles.

In preliminary testing, it surprisingly showed more pronounced CD spectral peaks compared to gammadion arrays described in literature. Hence, a logical mechanism behind its superior generation of superchiral fields and strong CD interaction was developed based on intuition (see Figure 2 and Figure 3) which was later verified by photonic simulation in Figure 13 and Figure 14.
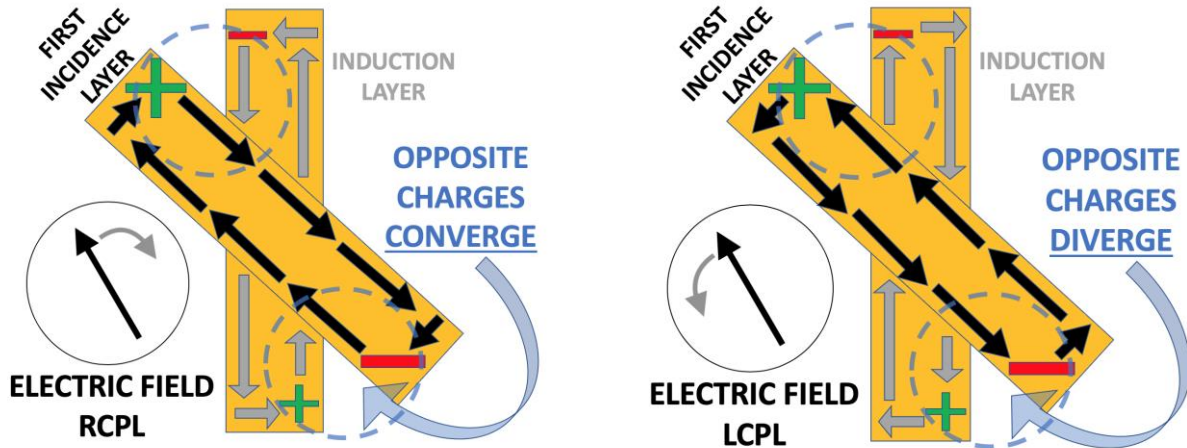
*(The red negative charges are the conduction electrons and green positive charges are the absence of conduction electrons in the positively charged gold ion lattice.)*

**Figure 2:** *Schematic Showing the Charge Circulation in a Simplified Woodpile Junction as a result of RCPL Propagating Through Woodpile, Into the Page.*

**Figure 3:** *Schematic Showing the Charge Circulation in a Simplified Woodpile Junction as a result of LCPL Propagating Through Woodpile, Into the Page.*

The fundamental reason behind the strong CD interaction shown by the woodpile nanostructure is the dissimilar collective charge movement that occurs when RCPL and LCPL impinge on it. There are two key conditions satisfied by the plasmonic nanostructure which allow this to function:

**1.2 The First Incidence Layer Exhibits a Stronger Plasmonic Resonance than the Induction Layer**

In the top-down view of a simplified woodpile junction presented in Figure 2 and Figure 3, linearly polarized light propagates into the page. The combined effect of having a larger surface area exposed and being in closer proximity to the source causes the impinging EM waves to have an overall stronger plasmonic interaction on the top layer (first incidence layer) compared to the bottom layer (induction layer). The former effect, of having a larger surface area, is more significant than its being closer to the source.

**1.3 The Woodpile Nanostructure Permits Asymmetricity in Charge Circulation to Manifest through its Chirality**

As seen in Figure 2 and Figure 3, the right-handed woodpile has no planes of mirror symmetry. To analyze how this chiral morphology induces asymmetrical absorption of RCPL and LCPL, we shall first consider RCPL impinging on the structure (see Figure 2) for which the

electric field vector in RCPL rotates clockwise. In both the first incidence layer and the induction layer, the conduction electrons are compelled to move in the direction opposite to the electric field vector, and since the electric field is rotating clockwise, the high electron density also rotates in the same clockwise fashion (denoted by the black arrows). However, by virtue of the stronger plasmonic interaction experienced by the first incidence layer due to its larger surface area (explained in 1.2), it also has a stronger charge circulation compared to the induction layer. Hence, this disparity in electric field strength would naturally cause the first incidence layer's charge rotation to induce a secondary charge rotation, in the induction layer (denoted by the grey arrows). However, this induced rotation would be in the counter-clockwise direction due to the principle of unlike charges attracting; a strong positive charge rotating clockwise in the first incidence layer attracts along an induced negative charge in the induction layer, which rotates counter-clockwise due to the chiral structure of the woodpile, intuitively presented in Figure 2. These rotations permit the attracting unlike charges to converge together, which makes it energetically favourable.

On the contrary, in Figure 3, the LCPL's counter-clockwise rotating electric field vector forces charges to rotate in a counter-clockwise direction. The manner of rotation does not permit the first layer charges to drag along the induced charges because the diverging nanowires restrict their movement and force them apart, shown in the dotted circles. This charge movement is unfavorable as work must be injected into the system to separate the attracting positive and negative charges. Hence, the weak plasmonic interaction produced by LCPL allows it to be transmitted relatively unimpeded, and the strongly interacting RCPL is absorbed to a larger extent. Also, do note that although the impinging LCPL generates an overall counter-clockwise rotation, the weak top-layer-induced clockwise rotation only creates a slight offset in the net rotation.

In summary, the chiral boundaries of the right-handed woodpile naturally favour a clockwise circulation of the low-mass electrons in the conduction band of the first induction layer, which the RCPL provides, so its strong interaction leads to greater absorption. On the other hand, LCPL is absorbed minimally due to the unfavourable charge circulations that it induces. This mechanism was postulated to underpin the asymmetrical absorption of RCPL and LCPL when linearly polarized light impinges on the structure, creating a pronounced CD spectrum.

This investigation shall proceed to optimize the dimensions of the woodpile structure while analyzing the results to verify the abovementioned hypothesized mechanism.

**Table 1:** *Classification of the Parameters Involved in this Investigation*

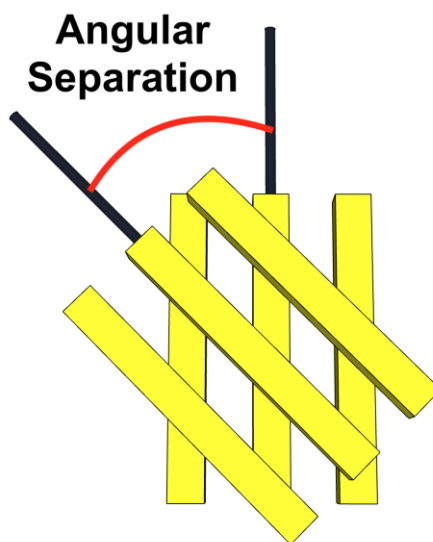| Independent Variables | Dependent Variable | Control Variables |
|---|---|---|
| 1. Angular Separation Between Layers (see Figure 4)<br><br>2. Number of Nanowire Layers (see Figure 5) | Circular Dichroism Spectrum | Material (Au)<br>Nanowire height (30 nm)<br>Nanowire thickness (30 nm)<br>Nanowire length (115 nm)<br>Number of nanowires per layer (3)<br>Wavelength of source (200 nm to 1000 nm) |



**Figure 4:** *Schematic Representation of the Clockwise Angular Separation Between the Parallel Nanowire Layers of a Woodpile Nanostructure (Independent Variable 1)*
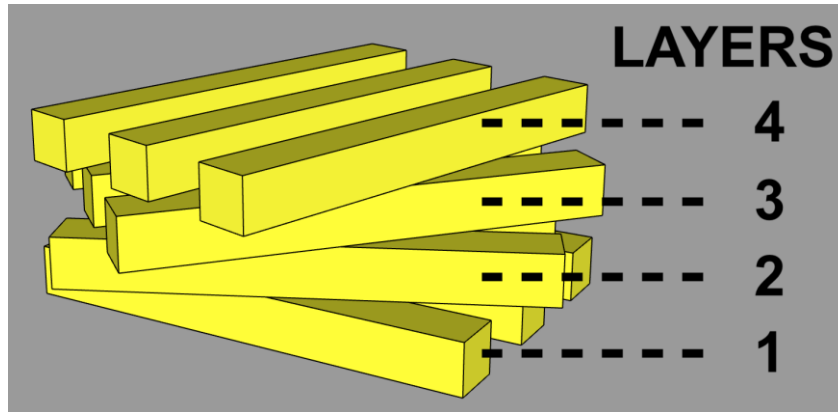
**Figure 5:** *Schematic Representation showing How the Number of Nanowire Layers in a Woodpile Nanostructure are Counted (Independent Variable 2)*

## 2. Procedures

A 3D Maxwell solver called FDTD Solutions, a nanophotonic simulation software that uses the finite-difference-time-domain method, allows us to model interactions of electromagnetic waves with metamaterials without necessitating actual CD spectroscopes. The simulation was configured as shown in Figure 6.
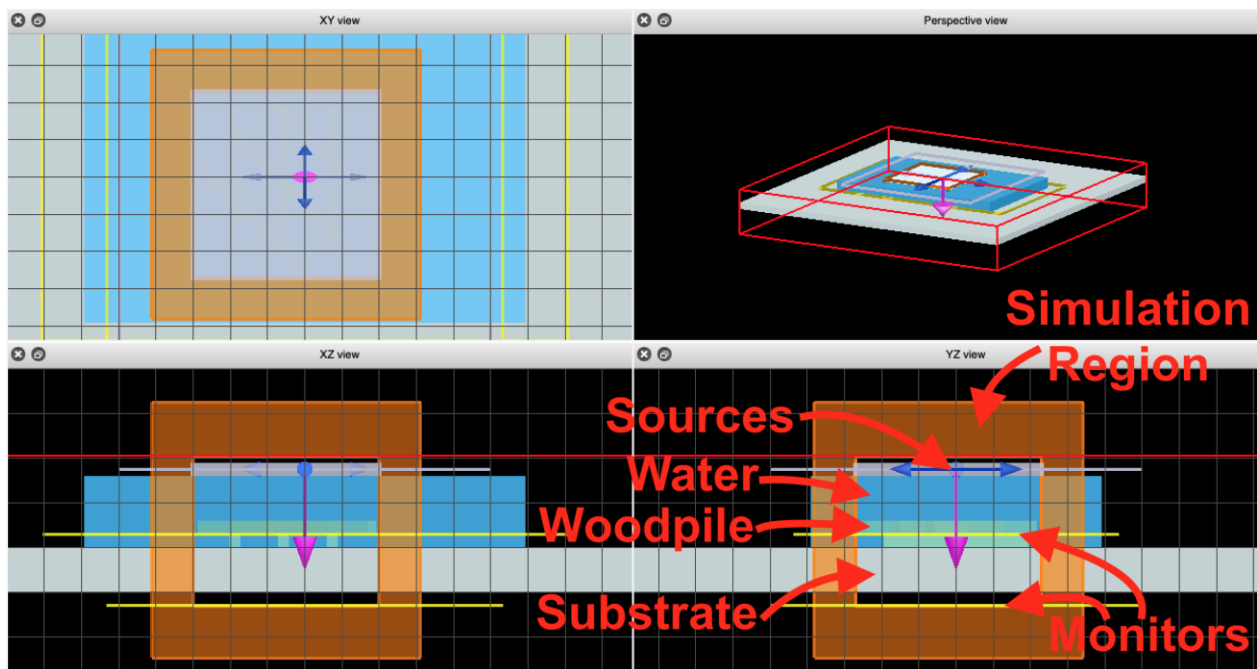


**Figure 6:** *FDTD Simulation Region Viewed Through Various Perspectives*

**Table 2:** *Details of all the Entities used the FDTD Simulation and their Corresponding Spatial Configuration and Settings (Continued on Page 9)*

| Entity | Spatial Configuration in Simulation Region | Specific Setting |
|---|---|---|
| FDTD Simulation Region | NA | Mesh Accuracy (5) <br> Simulation Temperature (300 K) <br> Boundary Conditions (PML) |
| Substrate | Lower half | Thickness (100 nm) <br> Material ($SiO_2$ (Glass) - Palik) |
| Woodpile Nanostructure | On the surface of the glass substrate | Material (Au (Gold) - Palik) |
| Water Submersion Layer (Representing buffer solution with enantiomers in suspension) | On the surface of the glass substrate, surrounding woodpile | Thickness (160 nm) <br> Material ($H_2O$ (water) – Palik) |
| Movie Monitor | Top surface/within woodpile | Resolution (1000 by 1000) <br> Field Component (Ez) <br> TM Field Component (Ez) <br> TE Field Component (Ey) |
| Frequency-Domain Field and Power Monitor | Beneath glass substrate | Default Settings |
| Right Circularly Polarized Light Source (Combination of two linearly polarized sources) | Above the water layer, z-axis injection (200 - 1000 nm) | Source 1: (Amplitude 1, Phase 0°, Polarization angle 0°) <br><br> Source 2: (Amplitude 1, Phase 90°, Polarization Angle -90°) |
| Left Circularly Polarized Light Source (Combination of two linearly polarized sources) | Above the water layer, z-axis injection (200 - 1000 nm) | Source 1: (Amplitude 1, Phase 0°, Polarization Angle 0°) <br><br> Source 2: (Amplitude 1, Phase 90°, Polarization angle 90°) |

The EM wave sources were set to 200-1000 nm because this paper deals with plasmonic modes. Vibrational plasmons existing below 200 nm are beyond the scope of this investigation.

## 3. Risk and Safety

Preclude setting excessively high mesh accuracy as the computer may overheat and stall, potentially resulting in damage to hardware.

## 4. Methods for Data Analysis

The simulation software only outputs the raw transmission data, taken at the location of the Frequency-Domain Field and Power Monitor, which must first be processed into useful information about the magnitude and location of the CD peaks. Firstly, the simulation is executed, separately for RCPL and LCPL and the transmission data for each circular polarization can be extracted using the Frequency-Domain Field and Power Monitor, allowing computation of the CD spectra. CD for a particular wavelength is conventionally given by; $Absorbance_{LCPL}(\lambda) - Absorbance_{RCPL}(\lambda)$ , but in terms of transmittance, it is; $Tranmittance_{RCPL}(\lambda) - Transmittance_{LCPL}(\lambda)$ . Thus, processing the transmittance data points for each discrete wavelength in the range and plotting gives the CD spectrum.

Since it was not possible to use the in-built optimization function in the software to optimize the parameters of the nanostructure between two independent simulations for RCPL and LCPL, the woodpile was optimized manually by making incremental changes to the angular separation and the layer count.

The movie monitor's electric field distribution data is trivially extracted from the software by way of a .mpg file. By progressing through the footage slowly, frame by frame, one may detect hotspots on the surface of the metamaterial where the superchiral field is comparatively strong. Moreover, the change in the electric field distribution, denoted by the colour of the pixels at each point on the two-dimensional representation (red for positive, blue for negative), shows the collective charge movement.

## 5. Experimental Section with Methods and Results

In the process of optimizing the nanostructure, to achieve maximum circular dichroic properties within the limits of feasible future fabrication, simulations for the CD spectra at various angular separations, incremented by 15°, were executed while keeping all other parameters as control variables. A range of angles between 0° and 90° were employed as data

collection beyond 90° would redundantly duplicate a reflected version of the results, as has been tested, due to the symmetricity of the nanostructure. Table 3 presents the simulation results.

**Table 3:** *CD Spectra for 3-Layered Woodpile at Various Angular Separations*
*(The red and green lines denote the transmission of RCPL and LCPL*
*respectively, and the blue lines represent the CD spectra)*

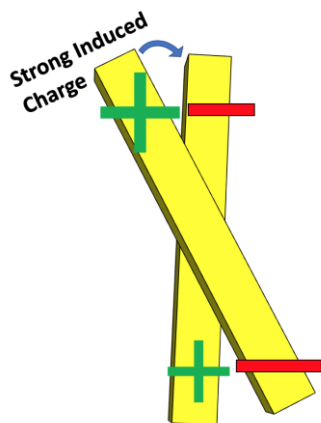| Angular Separation | CD Spectra | Angular Separation | CD Spectra |
|---|---|---|---|
| 0° |  | 60° |  |
| 15° |  | 75° |  |
| 30° |  | 90° |  |
| 45° |  | | |

**Figure 7:** *Schematic of Woodpile Charge Distribution at a Nanowire Junction for 30° Angular Separation showing Strong Induced Charges*
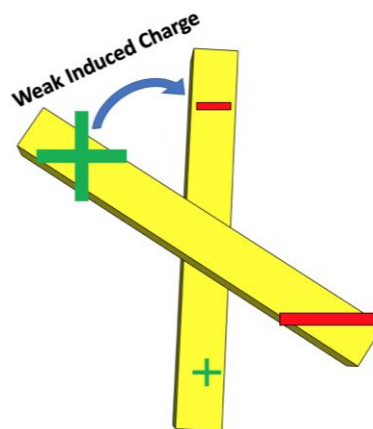
**Figure 8:** *Schematic of Woodpile Charge Distribution at a Nanowire Junction for 60° Angular Separation showing Weak Induced Charges*

At first glance, it may seem unintuitive that the CD at 30° and 60°, although being symmetrically angled from 45°, would have dissimilar CD spectra. However, since 60° is a wide angular separation, there is a more considerable distance between the charges on the nanowires on the topmost and nethermost layers. Thus, the induction rotation and the plasmon-plasmon coupling is weaker (see Figure 7 and Figure 8). For the 30° woodpile, the nanowires and therefore the charges are in close proximity, so the plasmons can couple more readily, which leads to a stronger 'p3' CD peak.

Nevertheless, all the CD peaks for the 30° woodpile are not as pronounced as that for 45° because the angle is not optimally large enough to evoke the most intense circulating charge motion which is significant in the asymmetric absorbance of the LCPL and the RCPL. Ergo, the CD spectra explicitly show that 45° yields the most amplified CD signal, with positive and negative peaks occurring at circa 740 nm and 795 nm and is the best compromise as the distance between the plasmons is not exceptionally long, but it concurrently provides enough of a wedge in the structure to create an effective division between the circulating charges in both layers.
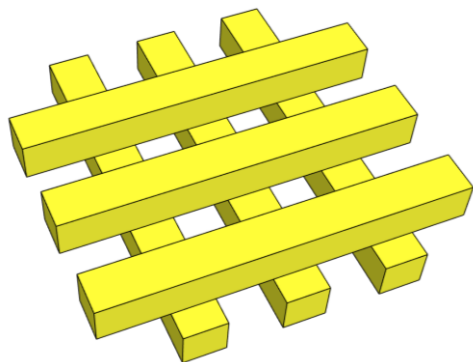
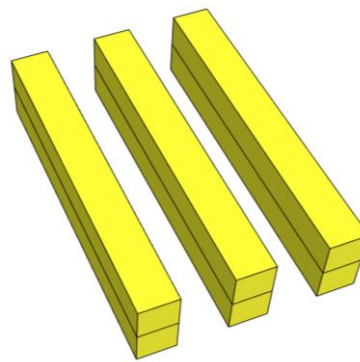**Figure 9:** 2-Layered *Achiral Woodpile Nanostructure with 90° Angular Separation*

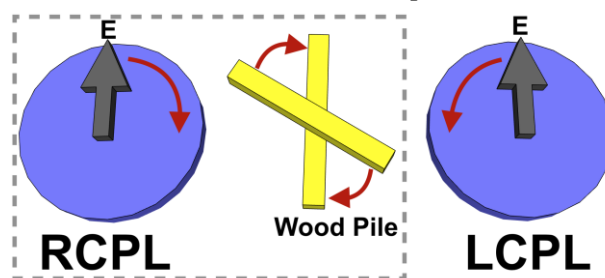**Figure 10:** 2-Layered *Achiral Woodpile Nanostructure with 0° Angular Separation*



**Figure 11:** *Schematic showing that RCPL Propagating into the Page has an Electric Field Vector Rotating in the Same Direction as the Structural Rotation of the Nanowires in the Woodpile*

With angular separations approaching 0° or 90°, the spectrum gets muted and nears zero because the woodpile nanostructure approaches an achiral state of 0° and 90° angular separation (see Figure 9 and Figure 10). Both structures have two planes of mirror symmetry, resulting in a reduced charge circulation, so it does not benefit from a strong CD interaction.

Notably, at 45°, since the structure is inherently right-handed, the positive CD peak ('p1') has a greater magnitude compared to the negative CD peak ('p2') because, agreeing with hypothesized the mechanism, the RCPL has a greater absorbance than the LCPL.

To determine the origination of the circular dichroic properties of the woodpile nanostructure, a simplified structure comprised of just two overlapping nanowire strands is simulated. The nanowire of first EM wave incidence is rotated 45° counter-clockwise with respect to the other to create a right-handed woodpile. Additionally, the nanowires have been made broader and thinner (like ribbons) to observe the lateral charge circulations better. A movie monitor is used to capture motion footage of the charge movements at the surface of the first incidence layer. Firstly, RCPL and LCPL of wavelength 740 nm are propagated through the

woodpile separately, because this is where the previously determined negative CD peak is located. Here the results are presented; Figure 13 and Figure 14 depict the electric field distributions for RCPL and LCPL at 740 nm (the positive CD peak 'p1)) and 795 nm (negative CD peak 'p2') for 45° angular separation.
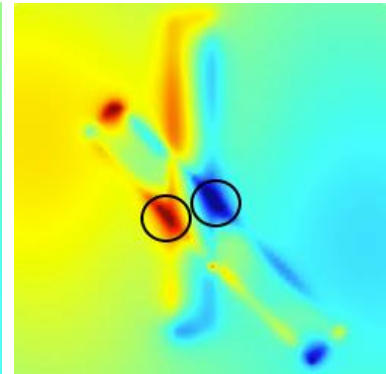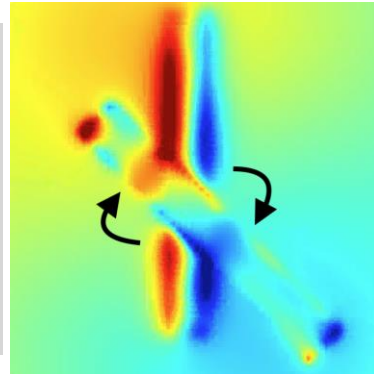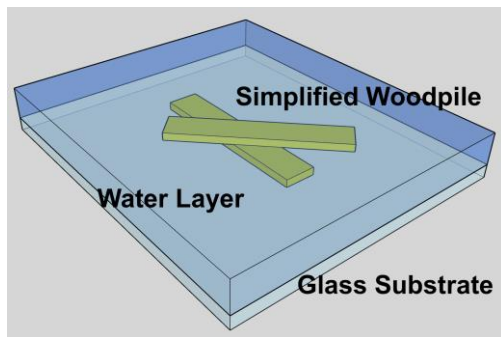


**Figure 12:** *Three-dimensional Representation of Simulation Region with Source Pointing Top-Down and the Movie Monitor below the Glass Substrate*

**Figure 13:** *RCPL*          **Figure 14:** *LCPL*

*Figure 13 and Figure 14 are Snapshots of the Movie Monitor Motion Footage Showing the Changing Electric Field Distribution During the Passage of 740 nm RCPL and LCPL Plane Waves Through the Woodpile Junction with 45° Angular Separation. (Red Denotes Negative Charge and Blue Denotes Positive Charge.)*
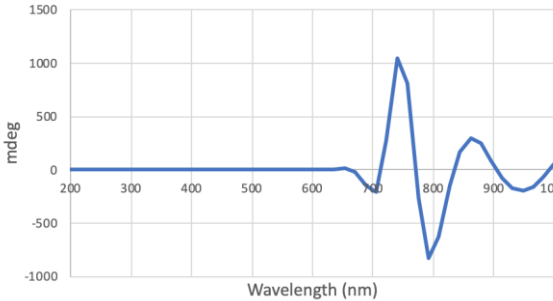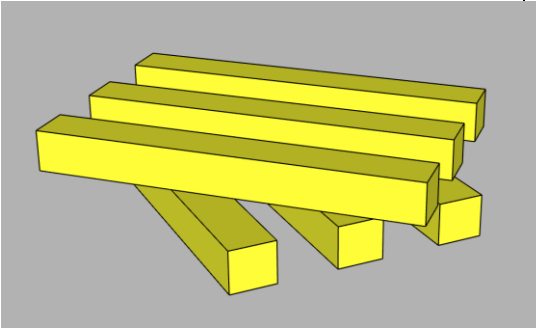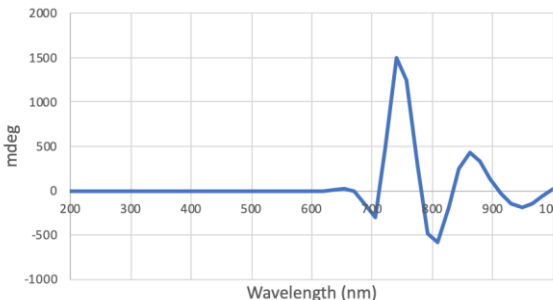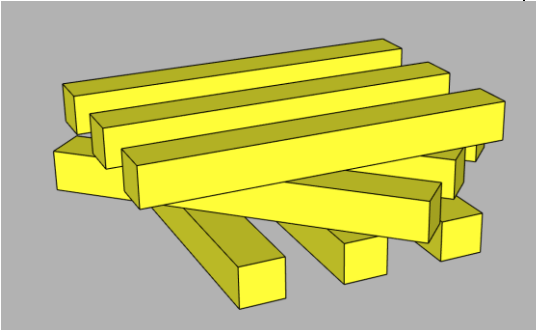
As explicitly shown by the black arrows in Figure 13, the RCPL's plasmonic interaction strongly correlates with the hypothesized model to an astonishing degree because the charges rotate clockwise in the first incidence layer, same as the electric field vector of the RCPL. It creates a 'vortex' of circulating electron density because its electric field rotation direction agrees with the right-handedness of the woodpile. On the other hand, the induction layer, although experiencing rotation in the same clockwise direction, has a weaker magnitude of charge movement which is again explained by the hypothesized induction rotation in the opposite direction, causing the counteraction. However, for the LCPL, it was not pre-conceived that the charges would pulsate stagnantly at the same points while constantly switching polarities, in the form of stationary surface plasmons. Nonetheless, the same mechanism may account for this because it stipulates that the right-handed chiral structure of the woodpile hinders the counter-clockwise charge circulation caused by the LCPL's electric field vector. Overall, this difference

in the nature of interaction between RCPL and LCPL gives rise to the stark asymmetricity in their respective absorbances.

Subsequently, these results lead to the postulation that the effect of the inter-layer induction would compound over multiple nanowire layers in the woodpile and create a more significant charge circulation disparity between RCPL and LCPL. For this reason, the possibility of improving the enhancement of the CD spectrum by increasing the number of nanowire layers in the woodpile was researched. The CD spectra for gold woodpiles of 30 nm nanowire thickness and 45° angular separation with increasing number of layers are presented in Table 4. The vertical axis is in mdeg units (a measure of elliptical polarization which is simply $\Delta Absorbance_{RCPL-LCPL}(\lambda) \times 32980$) for greater clarity and ease of comparison.

**Table 4:** *CD Spectra for Woodpiles with 45° Angular Separation at Various Layer Counts*

*(The red and green lines denote the transmission of RCPL and
LCPL respectively, and the blue lines represent the CD spectra)*

| Layer Count | CD Spectra for Woodpiles with 45° Angular Separation | 3D Representation of Woodpile |
|---|---|---|
| 2 |  |  |
| 3 |  |  |

| | | |
|---|---|---|
| **4** |  |  |
| **5** |  |  |
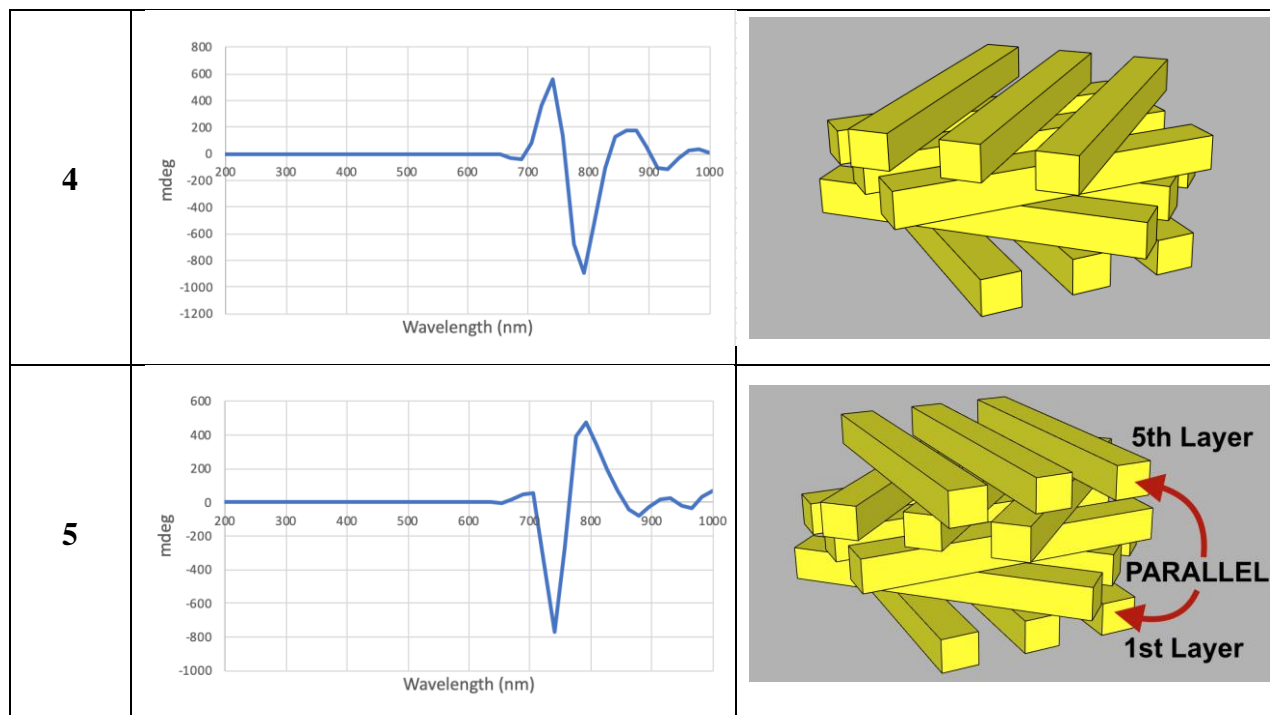
The first major positive CD peak reaches a maximum of 1502 mdeg with the 3-layer woodpile and then declines with subsequent layer additions. This correlates partially with the hypothesis which suggests that increased layer count would cause the induction to amplify the asymmetricity of charge circulation. However, beyond 3 layers, the CD peak decreases because additional layers cover more surface area and block more light, resulting in an overall decrease in transmission. Correspondingly, there is a diminished difference between the transmittance of LCPL and RCPL.

Peculiarly, the polarity of the first major CD peak switches when going from a woodpile with 4 layers to one with 5 layers. It is reasonable to attribute this to the parallel arrangement of the first and fifth layers in the 5-layer woodpile because the induction rotation of charges that propagates down the layers might cause the first and the fifth layer to have dissimilar rotations, and thus interfere with one another, yielding a different CD spectrum.
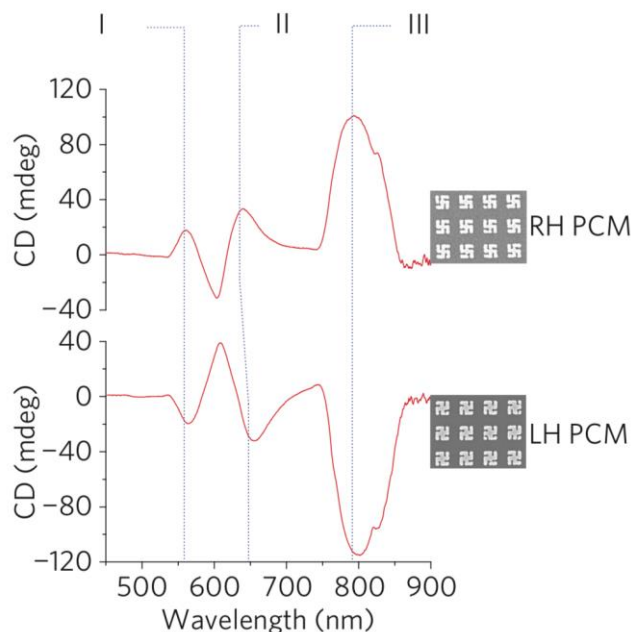
**Figure 15:** *Experimental CD Spectra of Gammadion Array from Literature (Hendry et al., 2010)*

Comparing the simulated woodpile's performance against the experimental CD spectrum of a chiral, right-handed gammadion array (see Figure 15) employed by a competitor paper, which yields a CD peak of magnitude 115 mdeg close to 800 nm, suggests that the woodpile shows a CD peak 1206 % larger than its counterpart, a vast improvement indeed.

## 6. Conclusion with Discussion of Results and Implications

The FDTD simulation has unequivocally verified the charge circulation mechanism which engenders the exceptionally strong plasmonic enhanced CD in the woodpile nanostructure. This knowledge provides deep insights into the generation of superchiral fields and potentially enables the creation of chiral metamaterials with stronger CD properties.

The woodpile, capable of producing a CD peak 1206 % larger than the gammadion array in the same wavelength region, advances the precision of plasmonic-enhanced CD spectroscopy, opening up possibilities to analyze lower sample concentrations, and to discover new spectral features previously unseen. Moreover, it enables the analysis of even smaller and lower-concentration analyte samples, unlike the conventional CD spectroscopy which requires thick analyte layers.

## 7. Future Research

- Attempt inserting dielectric spacers between the nanowire layers to impede charge flow between layers from diminishing the effect of charge induction.

- Since the relative orientation between the incident light and the plasmonic modes was kept constant throughout the investigation, one might attempt to impinge plane waves which are antiparallel to the chiral woodpile. Theoretically, this should not engender a stronger superchiral field as the woodpile is inherently an anisotropic material and the dissymmetry in the circulation of charges is most readily exploited when the plane waves are parallel to the nanowire layers.

- Since it is not possible to have a high CD at all wavelengths, one might attempt to tailor the woodpile nanostructure for specific chiral molecules by changing the thickness, spacing and shape of the nanowires. This would give control over the location of the CD peak and enable alignment with the natural maximum chiroptical effect shown by the enantiomers intended to be analyzed. This specialized drug detection technique would boost the CD and increase the resolution of spectral features while minimizing percentage error when determining enantiomeric excess.

- Fabricate the nanostructure to experimentally test the CD for comparison with the simulation data. Due to lack of access to such facilities, empirical trials could not be conducted for this paper. A potential method for fabrication is briefly outlined in Figure 16 and Figure 17.
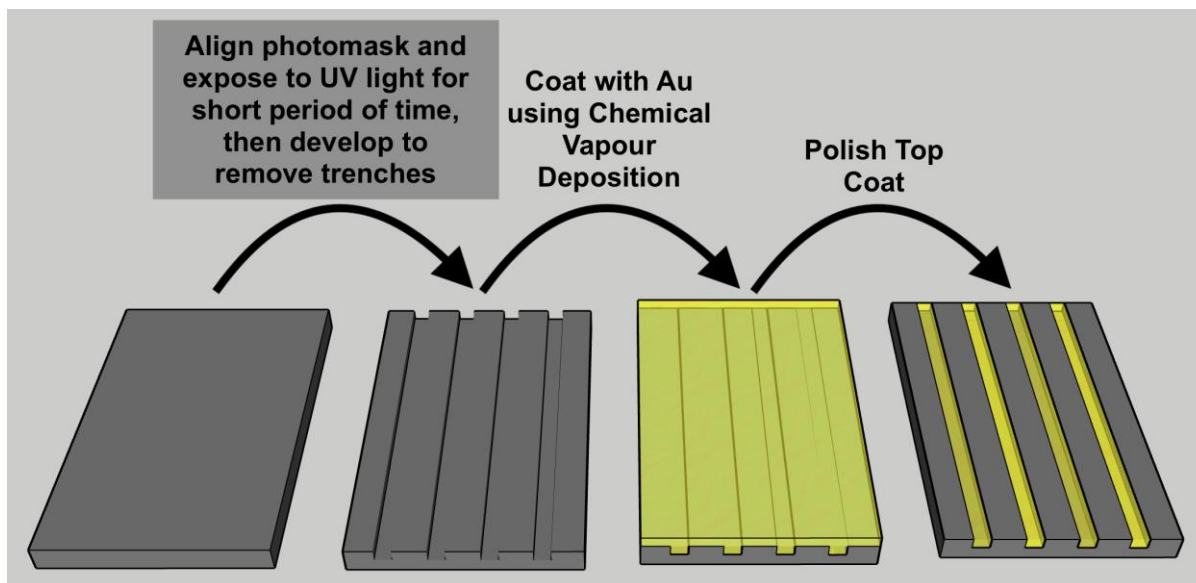


**Figure 16:** *Potential Method for Fabricating the Woodpile Nanostructure (Part 1)*
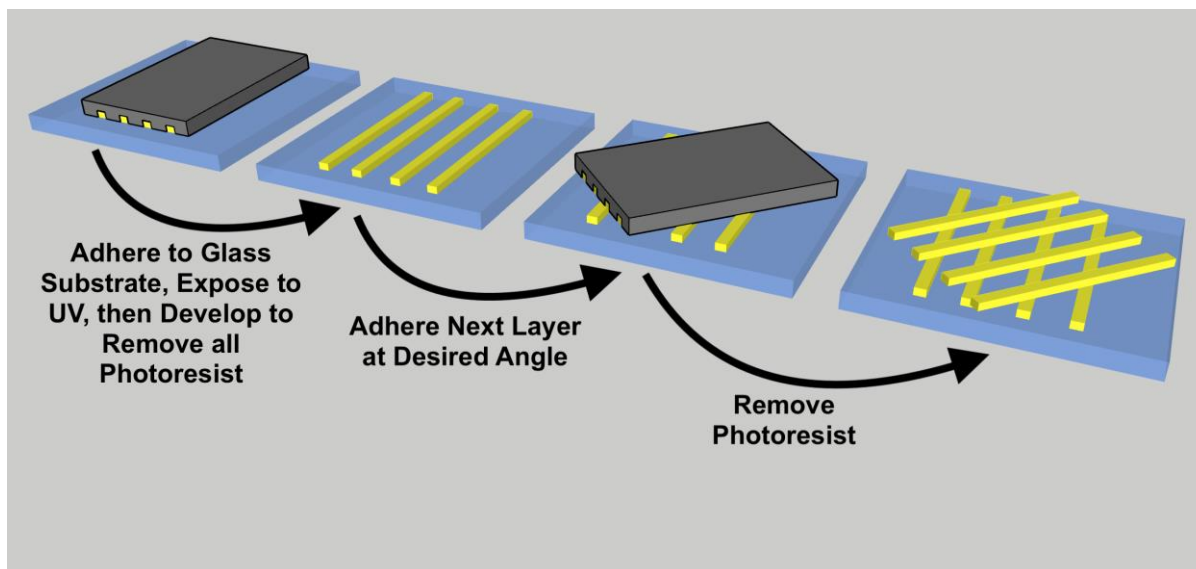
**Figure 17:** *Potential Method for Fabricating the Woodpile Nanostructure (Part 2)*

## 8. Limitations

- The mesh accuracy was reduced to level 3 to decrease simulation time down to 20 hours, but the number of frequency points used was sufficient to verify the hypothesis with confidence.

- Although the simulation suffices to observe the strength of the superchiral field generated by a nanostructure, it is not possible to realistically simulate the interaction between actual chiral molecules with the superchiral near-field generated by the woodpile. A practical experiment with CD spectroscopic tools and a fabricated nanostructure must be conducted to verify the simulation data, which only used a water layer to simulate the existence of a buffer solution with a suspension of chiral molecules.

- The numerical approach presented in this paper encompasses all the electromagnetic effects that may influence the enhancement of the CD signal of the assembly while neglecting other factors like charge transfer by chemisorbed analytes. Additionally, this paper focuses on the case in which molecular and plasmonic resonance are spectrally separated, which may not turn out to be the case when practical experiments are conducted.

- The simulation assumes that all chiral molecules are randomly oriented, so their CD interaction averages over all orientations, however, it might be that they take on a preferential orientation in the presence of the gold surface. This preferential orientation might yield different CD interactions.

## 9. Strengths

Normally, adsorbed chiral molecules at the gold surface take on a preferential orientation. However, in the case of the woodpile, the assumption that the chiral medium is homogenous and isotropic; meaning the chiral molecules take on a random molecular orientation and cancel out any anisotropic effects, is entirely acceptable as the chiral molecules completely surround the vertices of the nanowires. In other words, their orientation-related chiroptical effects nullify as they are all at random angles.

## References

Fan, Z., & Govorov, A. O. (2011). Helical Metal Nanoparticle Assemblies with Defects: Plasmonic Chirality and Circular Dichroism. *The Journal of Physical Chemistry C,115*(27), 13254-13261. https://doi.org/10.1021/jp204265x

Hendry, E., Carpy, T., Johnston, J., Popland, M., Mikhaylovskiy, R.V., Lapthorn, A.J., Kelly, S.M., Barron, L.D., Gadegaard, N., & Kadodwala, M. (2010). Ultrasensitive detection and characterization of biomolecules using superchiral fields. *Nature nanotechnology, 5 11*, 783-7. https://doi.org/10.1038/nnano.2010.209

International Union of Crystallography. (2016, October 5). Thalidomide: Understanding the purity and chirality of drugs and their metabolites. *ScienceDaily*. Retrieved May 12, 2019 from www.sciencedaily.com/releases/2016/10/161005114317.htm

Kuzyk, A., Schreiber, R., Fan, Z., Pardatscher, G., Roller, E., Högele, A., . . . Liedl, T. (2012). DNA-based self-assembly of chiral plasmonic nanostructures with tailored optical response. *Nature,483*(7389), 311-314. https://doi.org/10.1038/nature10889

Maoz, B. M., Chaikin, Y., Tesler, A. B., Elli, O. B., Fan, Z., Govorov, A. O., & Markovich, G. (2013). Amplification of Chiroptical Activity of Chiral Biomolecules by Surface Plasmons. *Nano Letters,13*(3), 1203-1209. https://doi.org/10.1021/nl304638a

Nguyen, L. A., He, H., & Pham-Huy, C. (2006). Chiral drugs: an overview. *International journal of biomedical science : IJBS*, *2*(2), 85–100.

Xia, Y., Zhou, Y., & Tang, Z. (2011). Chiral inorganic nanoparticles: Origin, optical properties and bioapplications. *Nanoscale,3*(4), 1374. https://doi.org/10.1039/c0nr00903b